Aghanejad A., et al., *BioImpacts,* 2018, 8(2), 117-127
doi: 10.15171/bi.2018.14
http://bi.tbzmed.ac.ir/

Mucin-1 aptamer-armed superparamagnetic iron oxide nanoparticles for targeted delivery of doxorubicin to breast cancer cells

Ayuob Aghanejad[1†], Hiwa Babamiri[1,2†], Khosro Adibkia[1,2], Jaleh Barar[1,2], Yadollah Omidi[1,2*]

[1] Research Center for Pharmaceutical Nanotechnology, Biomedicine Institute, Tabriz University of Medical Sciences, Tabriz, Iran
[2] Department of Pharmaceutics, Faculty of Pharmacy, Tabriz University of Medical Sciences, Tabriz, Iran

Article Info

Article Type:
Original Article

Article History:
Received: 31 Mar. 2018
Revised: 28 Apr. 2018
Accepted: 1 May 2018
ePublished: 5 May 2018

Keywords:
Breast cancer
Mucin-1 aptamer
Nanomedicine
SPION
Targeted drug delivery
Theranostics

Abstract

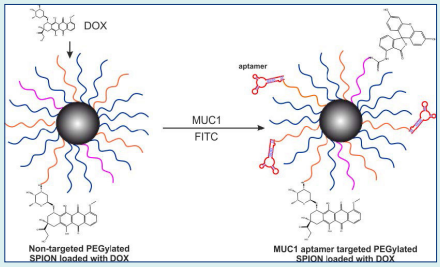

Introduction: Superparamagnetic iron oxide nanoparticles (SPIONs) can be functionalized with various agents (e.g., targeting and therapeutic agents) and used for targeted imaging/therapy of cancer. In the present study, we engineered doxorubicin (DOX)-conjugated anti-mucin-1 (MUC-1) aptamer (Ap)-armed PEGylated SPIONs for targeted delivery of DOX molecules to the breast cancer MCF-7 cells.

Methods: The SPIONs were synthesized using the thermal decomposition method and modified by polyethylene glycol (PEG) to maximize their biocompatibility and minimize any undesired cytotoxicity effects. Subsequently, DOX molecules were loaded onto the SPIONs, which were further armed with amine-modified MUC-1 aptamer by EDC/NHS chemistry.

Results: The morphologic and size analyses of nanoparticles (NPs) by transmission electron microscopy (TEM) and dynamic light scattering (DLS) revealed spherical and monodisperse MNPs with a size range of 5-64 nm. The FT-IR spectrophotometry and ^{1}HNMR analysis confirmed the surface modification of NPs. The cytotoxicity assay of the aptamer-armed MNPs exhibited a higher death rate in the MUC-1 over-expressing MCF-7 cells as compared to the MUC-1 under-expressing MDA-MB-231 cells. The flow cytometry analysis of the engineered Ap-armed SPIONs revealed a higher uptake as compared to the SPIONs alone.

Conclusion: Based on our findings, the anti-MUC-1 Ap-armed PEGylated SPIONs loaded with DOX molecules could serve as an effective multifunctional theranostics for simultaneous detection and eradication of MUC-1-positive breast cancer cells.

Introduction

Breast cancer is one of the high-prevalence malignancies among females with relatively high mortality worldwide. According to some global reports, approximately 1.7 million new cases of metastatic/advanced breast cancers are diagnosed each year.[1] To this end, a broad diversity of cancer detection approaches such as mammography, positron emission tomography (PET), single-photon emission computed tomography (SPECT) and magnetic resonance imaging (MRI) are used for the precise diagnosis and effective eradication of the malignant sites by improving the efficacy of cancer treatment modalities.[2-4] Currently, various imaging and therapeutic approaches are used for the treatment of breast cancer.[5-7]

It should be noted that some of the currently used conventional therapeutic modalities are invasive and may inadvertently induce undesired side effects in the other healthy organs, tissues and cells. Such complications need to be controlled by specifically targeting of the diseased cells/tissue with the nanoscaled targeted drug delivery systems (DDSs), the so-called multimodal nanomedicines and theranostics.[8]

In fact, for the selectively and specifically enhancing of the effects of chemotherapies on the target cells/tissue, a number of researchers have capitalized on the development of all-in-one seamless nanosystems (NSs) for simultaneous targeting, imaging, and treatment of cancer. For this purpose, several advanced nanoparticles (NPs) have been developed and further decorated with various targeting agents such as antibodies (Abs), aptamers (Aps)

*Corresponding author: Yadollah Omidi, Email: yomidi@tbzmed.ac.ir
† These authors contributed equally to this work and should be considered as the first co-authors.

© 2018 The Author(s). This work is published by BioImpacts as an open access article distributed under the terms of the Creative Commons Attribution License (http://creativecommons.org/licenses/by-nc/4.0/). Non-commercial uses of the work are permitted, provided the original work is properly cited.

or ligands as well as imaging agents such as radionuclides or fluorescent agents.[9,10]

So far, a large number of organic and inorganic NPs have been engineered and examined for their potential to serve as advanced nanoscaled DDSs. We have developed various NPs and NSs for targeted delivery of anticancer cytotoxic agents such doxorubicin (DOX), mitoxantrone (MTN), erlotinib (ELT), methotrexate (MTX), shikonin (SHK) and cisplatin (CDDP).[11-19] Among different types of NPs, magnetic nanoparticles (MNPs) and superparamagnetic iron oxide nanoparticles (SPIONs) possess distinct features, including biocompatibility, high surface area, magnetic resonance (MR) imaging, and contrasting capability. SPIONs are considered as one of the most attractive NPs to serve as a DDS of different anticancer pharmaceuticals.[20-23] In addition, they can be employed through either passive or active targeting mechanisms. Tumor cells, in coop with stromal cells, are able to form a permissive milieu, so-called tumor microenvironment (TME).

In solid tumors, anomalous biological phenomena occur within the TME, including aberrant metabolism of glucose and amino acids such as L-tryptophan by cancer cells, expression of several distinct molecular machineries by cancer cells, cooperation of the immune system with cancer cells, irregular angiogenesis with leaky endothelium and interstitial fluid with high pressure. The leaky tumor microvasculature (TMV) results in an enhanced permeability and retention (EPR) effect that is the basis of the passive targeting mechanism since NPs can accumulate within the TME through pores and gaps of endothelial cells of the TMV.[24-26]

In the active targeting mechanism, NPs such as SPIONs are armed with an appropriate homing agent (e.g., Ab, Ap, ligand), upon which the engineered NSs get an ability to target the diseased cells/tissues specifically. Various chemotherapy agents such as DOX, MTX, and CDDP can be loaded onto the NPs. These chemotherapies can induce profound toxicity in the human cells nonspecifically, while their formulation as nanoscaled targeted DDSs can significantly reduce their undesired toxicity and adverse reactions in the healthy cells/tissues.

Of the chemotherapy agents, DOX is an antineoplastic drug that is metabolized to doxorubicinol (DOXol), which is the major metabolite of DOX and can preferentially accumulate in the heart during the course of chronic administration of DOX, resulting in a profound cardiotoxicity. DOXol can interfere with iron by aconitase 1 and affect the regulation of calcium by interfering with Na^+/K^+ pumps of sarcoplasmic reticulum, F0F1 ATPase proton pump of mitochondria, ATP2A2 and Ryanodine receptor 2.[27-29] The interactions/regulations of DOX metabolites with the some of the normal functions of organs can result in some degrees of toxicity (e.g., cardiotoxicity).

Further, multidrug-resistance (MDR) can also be activated that may limit the clinical benefits of DOX.[30-33] On the verge of such undesired toxicity, many researchers have aimed at reducing the unwanted toxicity of DOX through the development of nanoformulation loaded with DOX molecules.

For the production of targeted nanoformulation, various cancer biomarkers have been exploited, including folate receptors and mucin 1 (MUC1). Of the cancer markers, MUC, as a well-studied transmembrane glycoprotein, shows at least 10-fold overexpression in most of the malignant adenocarcinomas such as breast cancer.[34] This transmembrane oncoprotein was shown to associate with the HER2-overexpressing breast cancer cells, and hence, functionalization of NPs with a MUC1 targeting ligand can result in the receptor-mediated endocytosis of NPs. The resultant targeted NPs can specifically interact with cancer cells, resulting in an increased intracellular concentration of drug molecules inside the cancerous cells.[35]

On the basis of these fundamental concepts, we prepared PEGylated SPIONs armed with an aptamer specific to MUC1. The nanoscaled targeted NS loaded with DOX was designed for the pH-triggered release of DOX molecules in the target cells, and hence, an evaluated cytotoxic impact on the human breast cancer MDA-MB-231 and MCF-7 cells.

Materials and Methods

Materials

N, N-dicyclohexylcarbodiimide (DCC), fluorescein isothiocyanate (FITC), N-hydroxysuccinimidde (NHS), poly(ethylene glycol) bis(carboxymethyl) ether-600 and poly(ethylene glycol) methyl ether 2000 were purchased from Sigma-Aldrich Chemie GmbH (Munich, Germany) and used *without* further purification. The human breast cancer, MCF-7, and MDA-MB-231 cell lines were obtained from National Cell Bank of Iran, Pasteur Institute (Tehran, Iran). All media and cell culture components were purchased from Invitrogen (Karlsruhe, Germany).

Aptamer (5′-NH2(C6)GGGAGACAAGAATAAACGCTCAAGCAGTTGATCCTTTGGATACCCTGGTTCGACAGGAGGCTCACAACAGGC-3′) was purchased from Takapoo Zist Co. (Tehran, Iran).

Instrumentation

Dynamic light scattering (DLS) and ξ-potential of the synthesized SPIONs were carried out using Nanotrac Wave (Microtrac Inc, Montgomeryville, PA, USA). The size and morphology were measured by a transmission electron microscope (TEM) Carl Zeiss, LEO 906E (Jena, Germany). The FT-IR analysis was performed using Bruker FT-IR, (Bruker Optik GmbH, Ettlingen, Germany) to confirm the functional group(s) in the range of 400–4000 cm^{-1}. The ^{1}HNMR spectra were recorded using 400 MHz spectrometer (Bruker Optik GmbH, Ettlingen, Germany). The UV/Vis analysis was performed using Cecil spectrophotometer (Cecil, Cambridge, UK) in the range of 200–800 nm.

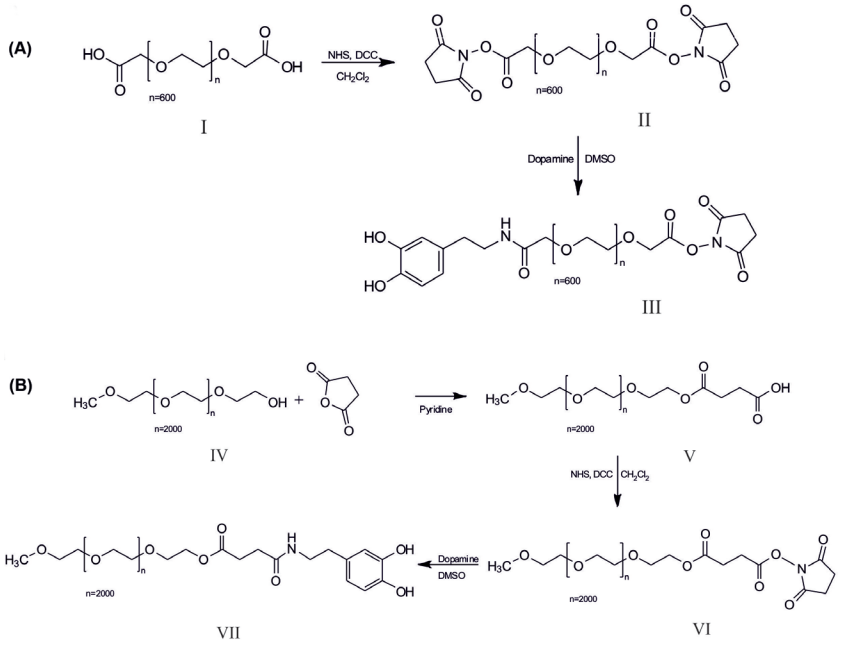

Fig. 1. Synthesis of DOPA-PEG_{600}-NHS (a) and DOPA-SA-PEG2000 (b). **I**, Poly(ethylene glycol) bis(carboxymethyl) ether-600; **II**, Poly(ethylene glycol) bis(carboxymethyl)-600 NHS ester (PEG600-2NHS); **III**, Dopamine-PEG_{600}-NHS (DOPA-PEG_{600}-NHS); **IV**, Poly(ethylene glycol) methyl ether 2000; **V**, poly(ethylene glycol) methyl ether 2000 succinic acid (PEG_{2000}-SA); **VI**, PEG_{2000}-SA-NHS ester (PEG_{2000}-SA-NHS); **VII**, Dopamine- PEG_{2000}-SA(DOPA-SA-PEG_{2000}).

Preparation of poly(ethylene glycol) bis(carboxymethyl)-600 NHS ester (PEG_{600}-2NHS)

The solution of *N,N'*-dicyclohexylcarbodiimide (0.667 g, 0.367 mmol) in dichloromethane (5 mL) was added dropwise to a stirred solution of poly(ethylene glycol) bis(carboxymethyl) ether-600 (1 g, 1.67 mmol) and *N*-hydroxysuccinimide (422 mg, 0.367 mmol) in 20 mL dichloromethane. The reaction mixture was stirred overnight at 25°C under the N_2 flow, then the mixture poured onto the pad of silica gel and eluted with n-hexane/ethyl acetate (8:2) to obtain PEG_{600}-2NHS (product II, shown in Fig. 1) as a yellow oil (1.2 g, 90%). The FT-IR ν^{max} (solution in CH_2Cl_2): 2948, 2876, 1772, 1706, 1656, 1545, 1431, 1354, 1213, 1083cm^{-1}.The ^{1}HNMR (400 MHz; $CDCl_3$): 2.7 (8H, m, NCO–CH_2–CH_2–CON), 3.75-377 (10H,–O–CH_2–CH_2–O–) and 4.16 (4H, s, –O–CH_2–COO–).

Synthesis of dopamine-PEG_{600}-NHS (DOPA-PEG_{600}-NHS)

Dopamine (DOPA) (184 mg, 1.2 mmol) was dissolved in 10 mL CH_2Cl_2, then the solution of PEG_{600}-2NHS (1 g, 1.2 mmol) in 10 mL CH_2Cl_2 was added. The mixture was stirred overnight at 25°C under the N_2 flow. The insoluble compounds were filtered, and then the filtrate was precipitated using diethyl ether. The yield of DOPA-PEG_{600}-NHS (product III, shown in Fig. 1) was 0.82 g (79%). The FT-IR ν^{max} (solution in CH_2Cl_2): 3441, 3997, 2914, 1657, 1422, 1210, 1031 cm^{-1}. The ^{1}HNMR (400 MHz; $CDCl_3$) 2.61 (2H, t,–CH_2–CH_2N–), 2.81 (4H, m, NCO–CH_2–CH_2–CON), 3.27 (2H, t, –Ph–CH_2–CH_2–), 3.36–3.63 (10H, –O–CH_2–CH_2–O–), 4.08 (2H, s, O–CH_2–CO-NH-), 4.26 (2H, t, O–CH_2–COO–N), 6.52 (1H, d, Ph) and 6.71 (2H, m, Ph).

Preparation of poly(ethylene glycol) methyl ether 2000 succinic acid (PEG_{2000}-SA)

The poly(ethylene glycol) methyl ether 2000 (9 g, 4.5 mmol) was dissolved in 20 mL pyridine, then succinic anhydride (SA) (2.25 g, 22.5 mmol) was added and the reaction mixture refluxed overnight under vigorous stirring. The solvent was evaporated under vacuum and the residue was extracted by dichloromethane and re-precipitated using diethyl ether. The yield of PEG_{2000}-SA was 7.46 g (79%). The FT-IR ν^{max} (solution in CH_2Cl_2): 2853, 1962, 1740, 1463, 1356, 953 cm^{-1}. The ^{1}HNMR (400 MHz; $CDCl_3$) 2.65 (2H, t, –COO–CH_2–CH_2–COO–), 2.87 (2H, t,–COO–CH_2–CH_2–COO–), 3.19 (3H, s, O–CH_3), 3.37–3.67 (34 H, –O–CH_2–CH_2–O–), 4.54 (2H, t, COO–CH_2–CH_2–O–).

Synthesis of PEG_{2000}-SA-NHS ester (PEG_{2000}-SA-NHS)

The solution of N,N'-dicyclohexylcarbodiimide (205 mg, 99.3 mmol) in dichloromethane (10 mL) was added dropwise to a stirred solution of PEG_{2000}-SA (2 g, 95.2 mmol) and N-hydroxysuccinimide (115 mg, 99.3 mmol) in 100 mL dichloromethane. After 24 hours, the mixture was filtered using a filter paper and purified using a pad of silica gel, which was then eluted with n-hexane/ethyl acetate (9:1) to obtain PEG_{2000}-SA-NHS (product VI, shown in Fig. 2), yield (1.56 g, 74%). The FT-IR ν^{max} (solution in CH_2Cl_2): 2879, 1731, 1459, 1345, 1100, 952 cm^{-1}. The ^{1}HNMR (400 MHz; $CDCl_3$) 2.63 (2H, t, –COO–CH_2–CH_2–COO–), 2.88 (4H, m, NCO–CH_2–CH_2–CON)

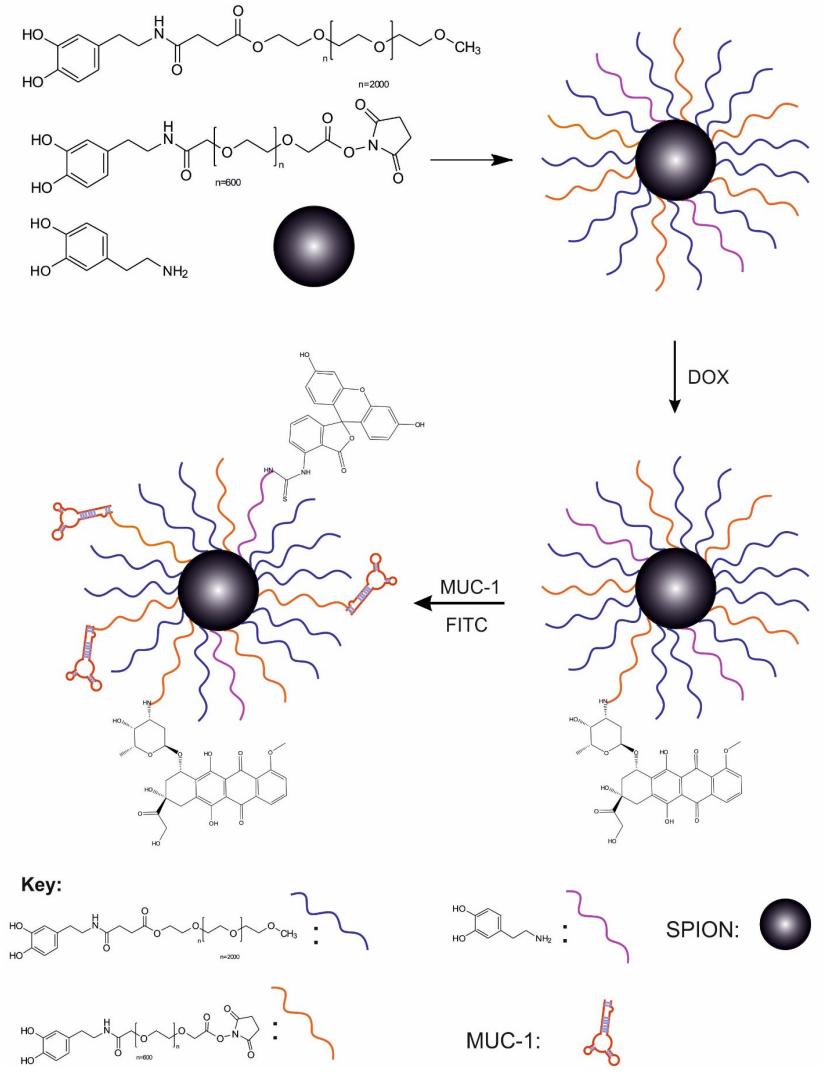

Fig. 2. Schematically represents preparation of magnetic nanopartciles.

2.91 (2H, t,–COO–CH_2–CH_2–COO–), 3.19 (3H, s, O–CH_3), 3.36–3.64 (34H, –O–CH_2–CH_2–O–), 4.54 (2H, t, COO–CH_2–CH_2–O–).

Synthesis of dopamine- PEG_{2000}-SA(DOPA-SA-PEG_{2000})

The solution of PEG_{2000}-SA-NHS (1 g, 45.15 mmol) in 10 mL CH_2Cl_2 was added to the solution of dopamine (70 mg, 45.2 mmol) and triethylamine (TEA) (10 µL) in 50 mL CH_2Cl_2. The mixture was stirred overnight at RT under the N_2 flow. The insoluble compounds were filtered and the filtrate was precipitated using diethyl ether. The yield of DOPA-PEG_{600}-NHS (product VII, shown in Fig. 2) was 0.85 g (83%). The FT-IR ν^{max} (KBr): 3404, 2887, 1719, 1019, 1425, 1227, 1657, cm^{-1}. The ^{1}HNMR (400 MHz; $CDCl_3$) 2.60 (2H, t, –Ph–$\underline{CH_2}$–CH_2–), 2.75 (4H, m, NCO–CH_2–CH_2–COO), 3.19 (3H, s, O–CH_3), 3.39 (2H, t,–CH_2–$\underline{CH_2}$NH–), 3.27 (2H, t, –Ph–CH_2–CH_2–), 3.5–3.63 (34H, –O–CH_2–CH_2–O–), 4.54 (2H, t, COO–$\underline{CH_2}$–CH_2–O–), 6.52 (1H, d, Ph) and 6.72 (2H, m, Ph).

Preparation of SPIONs

Iron (III) acetylacetonate ($Fe(acac)_3$) (0.11 g, 0.31 mmol) was dissolved in the mixture of oleylamine and benzyl ether (2 mL:2 mL) and dehydrated at 110°C for 1 hour under the N_2 flow. Then, the temperature of the reaction mixture was raised to 290°C for 3 hours under the N_2 flow. After cooling to the room temperature, 50 mL ethanol was added to the mixture and precipitated by centrifugation at 9000 ×*g* for 10-15 minutes.

The NPs were dispersed in 10 mL n-hexane and stored at 4°C. The yield was about 0.85 g (80%). The FT-IR ν^{max} (solution in CH_2Cl_2): 3473, 3011, 2919, 2853, 1772, 1738, 1650, 1543, 1455, 1298, 692, 453 cm^{-1}.[22]

SPIONs functionalization by DOPA, DOPA-PEG_{600}-NHS, and DOPA-SA-PEG_{2000}

The separate solutions of DOPA-PEG_{600}-NHS (50 mg), DOPA-SA-PEG_{2000} (100 mg), and dopamine (5 mg, 32.64 mmol) in 10 mL dichloromethane were added to a stirred suspension of SPIONs (40 mg) in 10 mL chloroform. The resulting mixture was sonicated at 25°C for 2 hours. Then, the PEG-modified NPs were precipitated by centrifuging at 5000 rpm for 15-20 minutes. The SPION-DOPA-PEG NPs rinsed using 10 mL ethanol (×3) and again was

centrifuged, and then, dispersed in 10 mL n-hexane and stored at 4°C. The yield was approximately 80%. The FT-IR ν^{max} (KBr): 3404, 3100, 2920, 2850, 1707, 1648, 1607, 1516, 1435, 1227, 1008, 706, 450 cm^{-1}.

Conjugation of a MUC-1 aptamer to MNPs (SPION-DOPA-PEG-DOX-MUC1)

About 100 nM of a solution of amine-terminated MUC1 aptamer in DNase/RNase free water was added to the suspension of NHS-activated SPION-DOPA-PEG-DOX (5mg/mL) in 2-(N-morpholino)ethanesulfonic acid (MES) buffer (pH = 7.4) and incubated under shaking with constant mixing at 25°C for 4 hours. Then, the MUC1 Ap-conjugated SPIONs were collected by the magnetic bead separation system and washed (×3) with phosphate buffered saline (PBS) and re-suspended in DNase/RNase free water at 4°C before use.

Conjugation of fluorescein isothiocyanate (FITC) to MNPs

For the conjugation of the fluorophore, the engineered SPIONs (100 mg) was suspended in 10 mL DMSO, and then, 20 µL of TEA was added to the suspension. Afterward, the solution of fluorescein isothiocyanate (FITC) (20 mg, 0.032 mmol) was added to the reaction flask and stirred at RT overnight under the N_2 flow. Finally, the product was collected using the magnetic bead separation system, washed with PBS (×3) and used for the cytotoxicity studies.

Chemical loading of DOX

The TEA (5 µL) was added to the suspension of SPION-DOPA-PEG (150 mg) in 10 mL of DMSO and the reaction mixture was stirred for 30 min under the N2 flow. In another flask, the solution of DOX (50 mg, 92 µmol) and TEA (5 µL) was stirred for 30 min. Then, these suspension and solution were mixed and stirred overnight at 25°C under the N_2 blanket. The engineered SPION-DOPA-PEG-DOX NPs were collected using the magnetic bead separation system. The loading efficiency was calculated by means of a calibration curve using a UV/vis spectrophotometer at 480 nm. (80%). The FT-IR ν^{max} (KBr): 3430, 3100, 2998, 2910, 2850, 1714, 1581, 1518, 1429, 1305, 1214, 1104, 1021, 708, 453 cm-1. Yield: 189 mg.

In vitro release studies

To evaluate the non-enzymatic release of DOX conjugated on MNPs, 2 mL of SPION-DOPA-PEG-DOX suspension (2.5 mg/mL) was placed into a pre-swollen dialysis bag (Sigma Aldrich, cut-off: 2000 Da). The suspended particles were immersed in 198 mL of PBS (pH 5.4, 6.4 and 7.4) and incubated at 37°C to confirm the pH-sensitive release trends of the NPs in the physiological condition. The incubation was continued for 240 hours. At the designated time points, the aliquots (2 mL) were taken out from the suspension while the total volume of media tank was kept constant by adding the same volume from fresh PBS after each sampling. The amount of released DOX from MNPs was estimated by a quantitative UV spectroscopy analysis at 480 nm and calculated according to the following equation: Loading efficiency (%)= [(amount of loaded DOX)/(amount of added DOX)]× %100.

Cell culture

The MCF-7 and MDA-MB-231 human breast cancer cells were cultured at a seeding density of 7.0×10^3 cells/well in Roswell Park Memorial Institute medium (RPMI-1640) supplemented with 10% fetal bovine serum (FBS) and streptomycin (100 mg/mL), penicillin (100 mg/mL), and L-glutamine (2 mM). The cells were kept at 37°C and 5% CO_2 in a water-saturated atmosphere in a CO2 incubator.

Cytotoxicity analysis

The toxicities of SPION-DOPA-PEG, SPION-DOPA-PEG-MUC1, free DOX, and DOX-loaded SPION-DOPA-PEG, as well as SPION-DOPA-PEG-MUC1 were investigated in the MCF-7 and MDA-MB-231 cells. About 24 hours post-seeding, the cells were treated with varying concentrations of NPs and drug-loaded NPs – equivalent to the DOX alone. At the designated time points (24, 48 and 72 hours of incubation periods), the media was removed and 50 µL (3-(4,5-dimethylthiazol-2-yl)-2,5diphenyltetrazolium bromide (MTT) solution (2 mg/mL in complete media) plus 150 µL of the fresh media were added to each well.[36] Then, the cells were incubated at 37°C for 4 hours, the media was removed and the formazan products formed by oxidation of the MTT dye were dissolved in DMSO (200 µL) plus Sorenson's buffer (40 µL). The absorbance of formazan product was read at 570 nm using a plate reader spectrophotometer, ELx808 (BioTek Instruments, Winooski, VT, USA).

SPIONs uptake evaluation by flow cytometry

The flow cytometry was used for the quantitative analysis of the cellular uptake of NPs by the MCF-7 and MDA-MB-231 cells. Briefly, six-well plates were seeded with a seeding density of 1.0×10^5 cells/well and incubated for 24 h. Then, the FITC-labeled MNPs dispersions were prepared under sterile conditions by diluting the stock in the corresponding FBS-supplemented growth media to the required concentration, immediately before their addition to the plates. The cultured cells were treated with the fluorophore-labeled non-targeted SPIONs, the Ap-conjugated SPIONs alone, and the DOX-loaded Ap-conjugated SPIONs at 37°C in a CO_2 incubator for 2 hours.[12,13] The cells were washed (×3) with PBS, and then, trypsinized, centrifuged at 160 ×g for 5 min. The cells pellet re-suspended in PBS and analyzed by FACS Calibur® flow cytometer (Becton Dickinson, San Jose, CA, USA) using a minimum number of 1.0×10^4 cells per event.

Statistical analysis

The results are expressed as the mean ± standard deviation (SD). The data were statistically assessed by the analysis of

variance (ANOVA) using GraphPad Prism 7.0 software (GraphPad Software Inc, San Diego, CA, USA). A *P* value of less than 0.05 was considered statistically significant.

Results

As shown in Figs. 1 and 2, for the development of the PEG_{600} and PEG_{2000} terminated dopamine molecules ($DOPA\text{-}PEG_{600}$, $DOPA\text{-}PEG_{2000}$) were synthesized through the amide bond. To increase the biocompatibility of NPs, SPIONs were functionalized with DOPA-PEG molecules via a ligand exchange reaction. Then, the functionalized SPIONs were loaded with DOX molecules and conjugated with the amine-modified MUC1 aptamer. After characterization of the engineered NSs by various techniques, in vitro cell experiments were conducted to study the biological impacts of the NSs.

FT-IR characterizations

The surface modifications of SPIONs with oleylamine and dopamine conjugated PEG were confirmed using FT-IR spectroscopy. The main peaks for oleylamine are: 3473 (NH_2), 3011(=C–H) and 2919, 2853(C–H) cm^{-1} and the peaks related to SPION are about 692, 453 (Fe–O) cm^{-1}. The peak at 1543 represents the Fe–N bond between NH_2 of oleylamine and Fe(III) of Fe_3O_4. Dopamine as an anchoring agent could replace the oleylamine on the surface of SPIONs.

The formation of SPION-DOPA-PEG NPs was validated by the presence of functional groups at 1008 (C–O–C, PEG), 2850, 2920 (CH_2), and the presence of phenyl ring of dopamine was confirmed by the peak at 3100 (=C–H). Moreover, the absorption peak at 1516 cm^1 indicates the amine functional group of dopamine. The results of 1500–1707 (–COO) and 1648 cm^1 confirm the conjugation of PEG-DOPA-NHS to the SPIONs. In the FT-IR spectrum of SPION-DOPA-PEG-DOX, the peak at 1581 cm^1 confirms the conjugation of NHS-activated PEG on the surface of SPIONs with DOX via the amide bonds (Fig. 3).

Morphological studies

A typical TEM image of the SPION-DOPA-PEG-DOX, as shown in Fig. 4, revealed a spherical shape with smaller size, which was further confirmed by the DLS. The slight difference between the TEM and DLS results may be due to the dehydration or attenuation of the NPs during the electron microscopy imaging process.

DLS analysis

The size and ξ-potential of synthesized MNPs attained by the DLS analysis resulted in a mean particle size of about 5±0.83 nm (PDI = 0.05) with a zeta potential of +25 mV for the engineered SPIONs alone.

The mean particle size of NPs was increased by the modification of SPIONs using DOPA-PEG, drug loading, and Ap conjugation processes. As a result, as presented in Fig. 4, the SPION-DOPA-PEG, SPION-DOPA-PEG-MUC1, SPION-DOPA-PEG-DOX and SPION-DOPA-PEG-DOX-MUC1 displayed the sizes about of 19±1.01 nm (PDI = 0.08), 21±1.83 nm (PDI = 0.07), 41±2.26 nm (PDI = 0.04) and 65±3.11 nm (PDI = 0.09), respectively. Additionally, the surface charge of all the NPs was found to be positive except the SPION-DOPA-PEG NPs because of containing carboxylic functional moieties on its surface.

Drug loading and release profile

For the loading of DOX molecules, the NHS-activated PEG600 was used for the conjugation of DOX onto the SPIONs through the formation of amide bonds. Further,

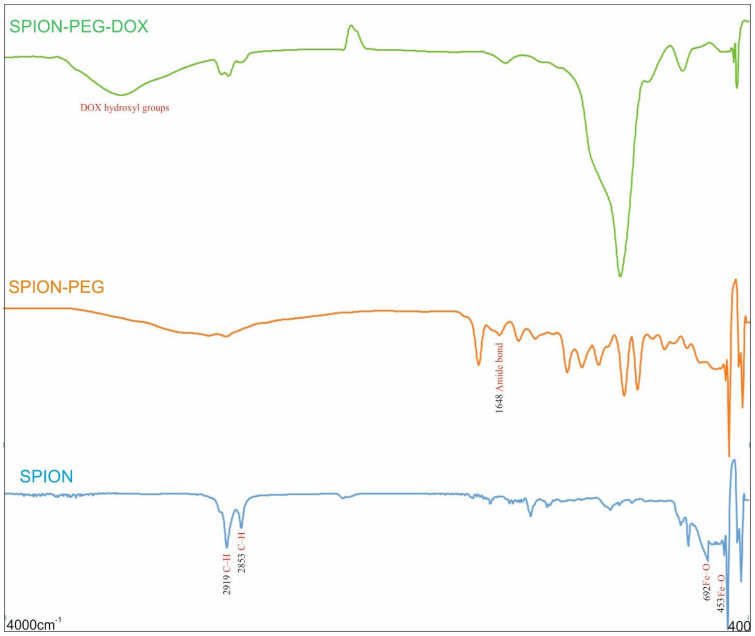

Fig. 3. FT-IR spectra of SPION, SPION-PEG, and SPION-PEG-DOX.

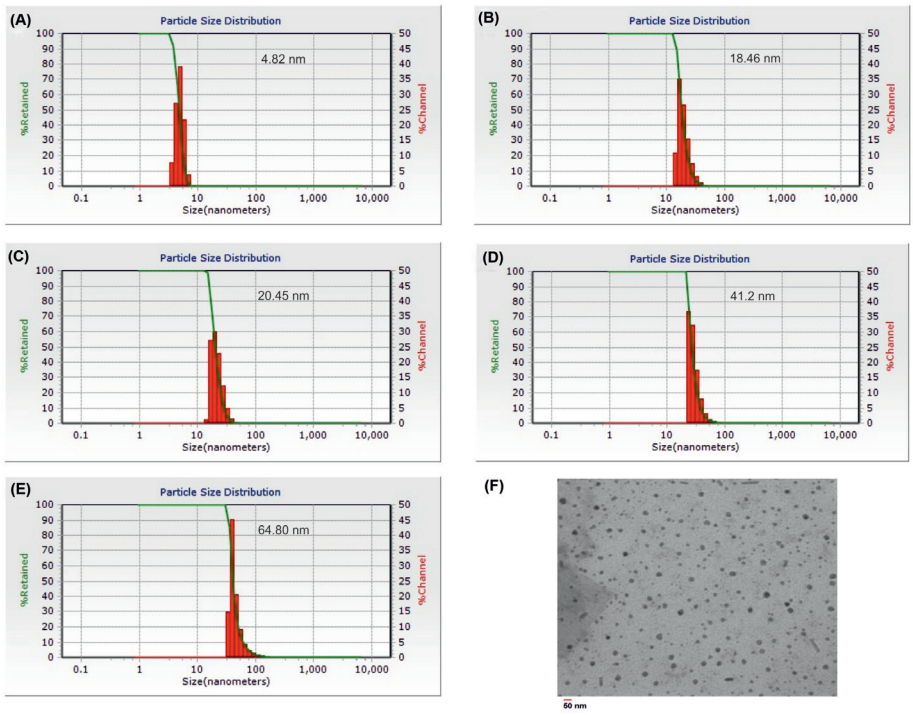

Fig. 4. The particle size of nanoparticles. (a) SPION. (b) SPION-DOPA-PEG. (c) SPION-DOPA-PEG-MUC1. (d) SPION-DOPA-PEG-DOX. (e) SPION-DOPA-PEG-DOX-MUC1. (f) Transmission electron microscopy image of SPION-DOPA-PEG-DOX.

because of the probability of interactions between the PEGylated SPIONs and DOX, some of the cargo loading capacity might be considered due to the physical loading. The results of drug release from NPs showed a pH-responsive behavior.

As shown in Fig. 5, the release of DOX molecules from NPs was found to be increased by reducing of the pH from the physiologic pH of 7.4 to the pH values of endosomal compartments (6.4 and 5.4).

Cytotoxicity effects of MNPs

The MTT assay confirmed the cytotoxicity of the prepared nanoformulations. As shown in Fig. 6, the cytotoxicity of the DOX-loaded PEGylated SPIONs were high in both

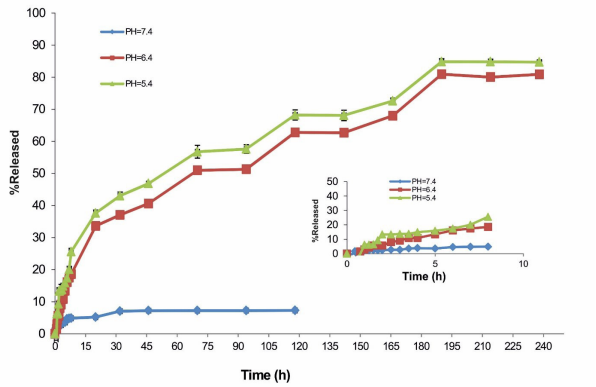

Fig. 5. Release of doxorubicin from SPION-DOPA-PEG-DOX-MUC1 nanoparticles based on UV absorption in buffer solutions (pH 5.4, 6.4, and 7.4 at 37ºC).

cell lines as compared to the free DOX.

The viability of the MUC1-high-expressing MCF-7 cells treated with SPION-DOPA-PEG-DOX-MUC1 NPs was considerably lower than that of the MUC1-low-expressing MDA-MB-231 cells. While DOX molecules alone induced a significant cytotoxicity in both cell lines, the SPION-DOPA-PEG-MUC1 and SPION-DOPA-PEG did not elicit noticeable cytotoxic effects even after 48 h in both MCF-7 and MDA-MB-231 cells. Expectedly, both treated cell lines were more viable at low concentrations of SPIONs alone while the cell viability was slightly decreased by the increase in the NPs concentration.

Of note, the DOX-loaded SPION-DOPA-PEG-MUC1 NPs exhibited an enhanced cytotoxicity in the MUC1-high-expressing MCF-7 cells as compared to the DOX molecules alone, but not in the MUC1-low-expressing MDA-MB-231 cells.

The cell viability study confirmed that the DOX-loaded SPION-DOPA-PEG-MUC1 NPs could induce significantly greater cytotoxicity in the MUC1-expressing MCF-7 cells. Moreover, under the same condition, the non-targeted DOX-loaded SPION-DOPA-PEG-MUC1 NPs showed lower toxicity than the targeted NPs in the MCF-7 cells, in large part due to the inefficient cellular uptake and relatively low release rate of the DOX molecules from the NPs.

FACS flow cytometry analysis of the cellular uptake

The cellular uptake of SPION-DOPA-PEG-DOX and Ap-conjugated NPs by the MUC1-high-expressing MCF-7

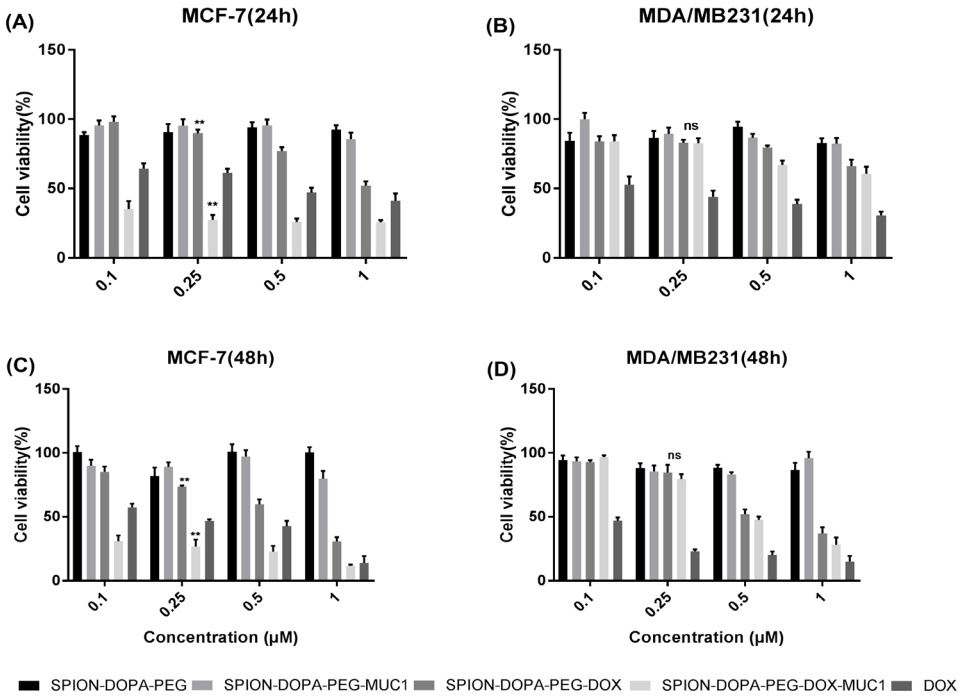

Fig. 6. The cell viability of the MUC1 high-expressing MCF-7 cells (panels a and c), and the MUC1 low-expressing MDA-MB-231 cells (panels b and d) after treatment with NPs. Cells were treated with different NPs, including SPION-DOPA-PEG, SPION-DOPA-PEG-MUC1, SPION-DOPA-PEG-DOX, SPION-DOPA-PEG-DOX-MUC1, and DOX for 24 and 48 h. ***P*< 0001, ns: not significant.

and the MUC-low-expressing MDA-MB-231 cells were further assessed by the flow cytometry method. As shown in Fig. 7, the MCF-7 cells treated with the SPIONs armed with Ap revealed a significantly enhanced internalization of NPs in these cells as compared to the non-targeted SPIONs.

Discussion

Solid tumors, as complex systems, show unique characteristics such as adaptation and evolution. The cancer cells get the capability of forming lenient microenvironment (TME), in which they are in some sort of coop with the immune system's cells and the other stromal components.[8,24] In fact, one single cancerous

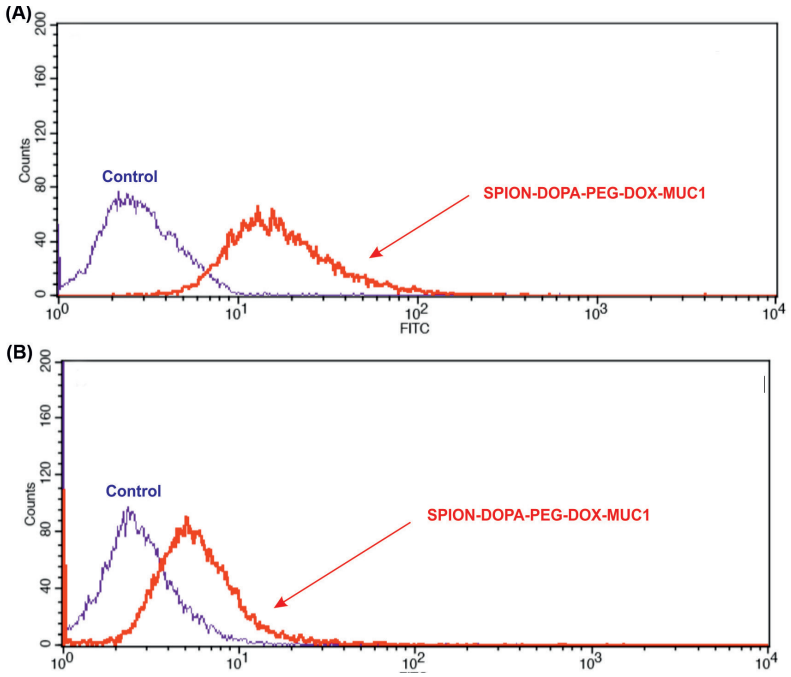

Fig. 7. Cellular uptake of SPION-DOPA-PEG-DOX-MUC1 nanoparticles by the MUC1 high-expressing MCF-7 cells (panel a) and the MUC1 low-expressing MDA-MB-231 cells (panel b). Cells were treated with NPs at the concentration of 10 μM for 2 h.

cell can evolve expressing different biological traits, which continue during its development to a number of cancerous cells and finally the formation of TME. Further progression of cancer may result in its invasion and metastasizing to neighboring cells and tissues. During this process, the epithelial cancer cells undergo a transition towards the formation of mesenchymal type cells (the so-called cancer stem cells). The emergence of such capacity bestows a single cancer stem cell great capability of invading other tissues with a great potential of avoiding anoikis – a programmed cell death process that occurs in the unanchored detached cells.[26, 37-39] Upon the treatment with anticancer chemotherapy, the cancer cells are further evolved, emerging the drug-resistance potential by the overexpression of molecular machineries such as MDR and multidrug resistance proteins (MRPs). Of particular relevance to the breast cancer chemotherapies include the functional expression of efflux machineries, including P-glycoprotein (P-gp), MRPs, and breast cancer resistance protein (BCRP). It has been reported that over 80% of currently used anticancer drugs are subjected to these efflux transporters.[40,41] The good news, however, is that the anticancer nanomedicine formulations show a great capability of overcoming such drug resistance potential of cancer cells.[42-44] If equipped with the targeting agents (Ab, Ap or ligand), the targeted nanomedicines can specifically/selectively detect the cancer cells and deliver the anticancer drugs to the diseased cells per se.[45-47] Once decorated with imaging agents, the targeted nanomedicines can be used for simultaneous diagnosis and therapy of cancer – a platform so-called diapeutics or theranostics.[8] We have previously developed and evaluated various types of nanoscaled DDSs using organic and inorganic entities, which have shown promising diagnostic and/or therapeutic outcomes.[48-51]

Our previous results on the MUC1 Ap-armed gold coated SPIONs highlighted the usefulness of these advanced NPs for the magnetic resonance (MR) imaging and photothermal therapy (PTT) of the colon cancer.[20] In this current study, we aimed at using Ap-decorated DOX-loaded PEGylated SPIONs for the targeted MR-imaging and specific delivery of cargo molecules to the diseased cells. The central focus of the current study was to develop an Ap-conjugated PEGylated SPIONs loaded with DOX (Figs. 1 and 2) for the targeted delivery of drug molecules to the breast cancer cells overexpressing the MUC1 molecular marker. The synthesis of NPs was carried out by the preparation of DOPA-PEG_{600}-NHS (50 mg) and DOPA-SA-PEG_{2000}, which were then grafted to SPIONs synthesized using $Fe(acac)_3$. The PEG_{600} di-acid was functionalized for the conjugation of MUC-1 and DOX molecules onto the SPIONs via dopamine. Moreover, on the account of the capability of PEG as a hydrophilic polymer in minimizing the possibility of NPs interactions with cells, we functionalized SPIONs with PEG_{2000} to solubilize NPs and reduce the undesired immune clearance of NPs by the reticuloendothelial system (RES). The engineered NPs were then grafted with MUC1 aptamer and loaded with DOX molecules (SPION-DOPA-PEG-DOX-MUC1 NPs). The resultant NS was characterized (Figs. 3 and 4) and examined for the release of DOX molecules from cargo NPs. The results revealed a faster release of DOX molecules from the SPION-DOPA-PEG-DOX-MUC1 NPs with a size of around 65 nm in an acidic media (Fig. 5). This finding confirms that the drug release might occur significantly in the endosomal compartment after the internalization of NPs via vesicular trafficking. We have previously discussed the cellular trafficking of NPs.[52] Further, the MUC1-mediated internalization has been shown to occur via clathrin-coated pits endocytosis as a dynamin- and Rab5-dependent process.[53,54]

The use of SPION-DOPA-PEG-DOX-MUC1 NPs against the MUC1-overexpressing breast cancer MCF-7 cells and the MUC1-underexpressing MDA-MB-231 cells revealed a markedly high internalization and toxicity in the MUC1-overexpressing MCF-7 cells, but not the MUC1-underexpressing MDA-MB-231 cells (Figs. 6 and 7).

Further, based on the internalization and cytotoxicity, the MUC1-high-expressing MCF-7 cells showed a significant difference between the uptakes of the targeted and non-targeted SPIONs. However, the MUC1-underexpressing MDA-MB-231 cells showed no significant difference between the cellular uptakes of the targeted and non-targeted SPIONs. It seems that targeted delivery through the MUC1 provides compelling evidence for the active targeting of the cancer cells that overexpress the MUC1 oncomarker. In accordance with our findings, it has been reported that the MUC1 Ap-armed mesoporous silica NPs can effectively target the breast cancer cells.[55] Further, the MUC1-Ap functionalized hybrid NPs have successfully been used for the targeted delivery of miRNA-29b to the non-small cell lung cancer.[56] Altogether, based on our findings, it can be speculated that the anti-MUC1 Ap-armed PEGylated SPIONs can be specifically taken up by the MUC1-positive cancer cells through clathrin-coated pits endocytosis, upon which the anticancer cargo molecules are delivered to the cancerous cells exclusively. As a result, the engineered nanosystem is envisioned to impose maximum therapeutic effect with minimum side effects in the solid tumors such as breast cancer.

Conclusion

In the current study, for the first time, we report on the development of PEGylated SPIONs armed with MUC1 aptamer and loaded with DOX molecules. The engineered SPION-DOPA-PEG-DOX-MUC1 NS showed significant targeting efficiency in the MUC1-overexpressing breast cancer cells, at which it might serve as a promising theranostic modality for the active targeting, imaging, and therapy of the breast cancer and other solid tumors that overexpress the MUC1 oncomark. Based on our results, the engineered targeted SPION-DOPA-PEG-DOX-MUC1 nanosystem indicated a high potential application

Research Highlights

What is current knowledge?

√ Superparamagnetic iron oxide nanoparticles (SPIONs) are functionalized with homing devices and loaded with chemotherapy agents to serve as nanoscaled theranostics.
√ Targeted SPIONs have been used for imaging and targeted therapy of solid tumors.

What is new here?

√ Anti-MUC-1 aptamer-armed PEGylated SPIONs loaded with doxorubicin could serve as an effective multifunctional theranostics for simultaneous detection and eradication of MUC-1-positive cancerous cells in various solid tumors such as breast cancer.

against cancer. The engineered nanosystem is envisioned to impose maximum therapeutic effect with minimum side effects in the solid tumors such as breast cancer. As a result, this NS may be considered as a promising theranostic nanoplatform for the clinical application against MUC1-overexpressing cancer cells.

Ethical approval

Not applicable to this study.

Competing interests

None to be declared.

Acknowledgment

The authors like thank all the members of the Research Center for Pharmaceutical Nanotechnology, Biomedicine Institute, Tabriz University of Medical Sciences for their support during this study.

Funding

This work was financially and technically supported by the National Institute for Medical Research Development of Iran (Grant No: 958333).

References

1. Wood R, Mitra D, de Courcy J, Iyer S. Patient-reported Quality of Life and Treatment Satisfaction in Patients With HR+/HER2- Advanced/Metastatic Breast Cancer. *Clin Ther* **2017**; 39: 1719-28. doi:10.1016/j.clinthera.2017.07.009
2. Mirzaei A, Jalilian AR, Aghanejad A, Mazidi M, Yousefnia H, Shabani G, et al. Preparation and Evaluation of (68)Ga-ECC as a PET Renal Imaging Agent. *Nucl Med Mol Imaging* **2015**; 49: 208-16. doi:10.1007/s13139-015-0323-7
3. Aghanejad A, Jalilian AR, Ardaneh K, Bolourinovin F, Yousefnia H, Samani AB. Preparation and Quality Control of (68)Ga-Citrate for PET Applications. *Asia Ocean J Nucl Med Biol* **2015**; 3: 99-106.
4. Mirzaei A, Jalilian AR, Badbarin A, Mazidi M, Mirshojaei F, Geramifar P, et al. Optimized production and quality control of (68)Ga-EDTMP for small clinical trials. *Ann Nucl Med* **2015**; 29: 506-11. doi:10.1007/s12149-015-0971-9
5. Vahidfar N, Jalilian Amir R, Fazaeli Y, Aghanejad A, Bahrami-Samani A, Alirezapour B, et al. Development of radiolanthanide labeled porphyrin complexes as possible therapeutic agents in beast carcinoma xenografts. Radiochimica Acta2014. p. 659.
6. Aghanejad A, Jalilian AR, Fazaeli Y, Beiki D, Fateh B, Khalaj A. Radiosynthesis and biodistribution studies of [62Zn/62Cu]–plerixafor complex as a novel in vivo PET generator for chemokine receptor imaging. *Journal of Radioanalytical and Nuclear Chemistry* **2014**; 299: 1635-44. doi:10.1007/s10967-013-2822-2
7. Aghanejad A, Jalilian AR, Fazaeli Y, Alirezapoor B, Pouladi M, Beiki D, et al. Synthesis and Evaluation of [(67)Ga]-AMD3100: A Novel Imaging Agent for Targeting the Chemokine Receptor CXCR4. *Sci Pharm* **2014**; 82: 29-42. doi:10.3797/scipharm.1305-18
8. Omidi Y. Smart Multifunctional Theranostics: Simultaneous Diagnosis and Therapy of Cancer. *Bioimpacts* **2011**; 1: 145-7. doi:10.5681/bi.2011.019
9. Same S, Aghanejad A, Akbari Nakhjavani S, Barar J, Omidi Y. Radiolabeled theranostics: magnetic and gold nanoparticles. *Bioimpacts* **2016**; 6: 169-81. doi:10.15171/bi.2016.23
10. Barar J, Omidi Y. Surface modified multifunctional nanomedicines for simultaneous imaging and therapy of cancer. *Bioimpacts* **2014**; 4: 3-14. doi:10.5681/bi.2014.011
11. Bakhtiary Z, Barar J, Aghanejad A, Saei AA, Nemati E, Ezzati Nazhad Dolatabadi J, et al. Microparticles containing erlotinib-loaded solid lipid nanoparticles for treatment of non-small cell lung cancer. *Drug Dev Ind Pharm* **2017**; 43: 1244-53. doi:10.1080/03639045.2017.1310223
12. Fathi M, Sahandi Zangabad P, Barar J, Aghanejad A, Erfan-Niya H, Omidi Y. Thermo-sensitive chitosan copolymer-gold hybrid nanoparticles as a nanocarrier for delivery of erlotinib. *Int J Biol Macromol* **2018**; 106: 266-76. doi:10.1016/j.ijbiomac.2017.08.020
13. Fathi M, Zangabad PS, Aghanejad A, Barar J, Erfan-Niya H, Omidi Y. Folate-conjugated thermosensitive O-maleoyl modified chitosan micellar nanoparticles for targeted delivery of erlotinib. *Carbohydr Polym* **2017**; 172: 130-41. doi:10.1016/j.carbpol.2017.05.007
14. Ranjbar-Navazi Z, Eskandani M, Johari-Ahar M, Nemati A, Akbari H, Davaran S, et al. Doxorubicin-conjugated D-glucosamine- and folate- bi-functionalised InP/ZnS quantum dots for cancer cells imaging and therapy. *J Drug Target* **2018**; 26: 267-77. doi:10.1080/1061186x.2017.1365876
15. Nakhlband A, Barar J, Bidmeshkipour A, Heidari HR, Omidi Y. Bioimpacts of anti epidermal growth factor receptor antisense complexed with polyamidoamine dendrimers in human lung epithelial adenocarcinoma cells. *J Biomed Nanotechnol* **2010**; 6: 360-9.
16. Hamidi A, Rashidi MR, Asgari D, Aghanejad A, Davaran S. Covalent immobilization of trypsin on a novel aldehyde-terminated PAMAM dendrimer. *Bulletin of the Korean Chemical Society* **2012**; 33: 2181-6.
17. Vandghanooni S, Eskandani M, Barar J, Omidi Y. Recent advances in aptamer-armed multimodal theranostic nanosystems for imaging and targeted therapy of cancer. *Eur J Pharm Sci* **2018**; 117: 301-12. doi:10.1016/j.ejps.2018.02.027
18. Matthaiou EI, Barar J, Sandaltzopoulos R, Li C, Coukos G, Omidi Y. Shikonin-loaded antibody-armed nanoparticles for targeted therapy of ovarian cancer. *Int J Nanomedicine* **2014**; 9: 1855-70. doi:10.2147/ijn.s51880
19. Shakoori Z, Ghanbari H, Omidi Y, Pashaiasl M, Akbarzadeh A, Jomeh Farsangi Z, et al. Fluorescent multi-responsive cross-linked P(N-isopropylacrylamide)-based nanocomposites for cisplatin delivery. *Drug Dev Ind Pharm* **2017**; 43: 1283-91. doi:10.1080/03639045.2017.1313859
20. Azhdarzadeh M, Atyabi F, Saei AA, Varnamkhasti BS, Omidi Y, Fateh M, et al. Theranostic MUC-1 aptamer targeted gold coated superparamagnetic iron oxide nanoparticles for magnetic resonance imaging and photothermal therapy of colon cancer. *Colloids Surf B Biointerfaces* **2016**; 143: 224-32. doi:10.1016/j.colsurfb.2016.02.058
21. Barar J, Kafil V, Majd MH, Barzegari A, Khani S, Johari-Ahar M, et al. Multifunctional mitoxantrone-conjugated magnetic nanosystem for targeted therapy of folate receptor-overexpressing malignant cells. *J Nanobiotechnology* **2015**; 13: 26. doi:10.1186/s12951-015-0083-7
22. Heidari Majd M, Asgari D, Barar J, Valizadeh H, Kafil V, Abadpour A, et al. Tamoxifen loaded folic acid armed PEGylated magnetic nanoparticles for targeted imaging and therapy of cancer. *Colloids Surf B Biointerfaces* **2013**; 106: 117-25. doi:10.1016/j.colsurfb.2013.01.051
23. Heidari Majd M, Asgari D, Barar J, Valizadeh H, Kafil V, Coukos

G, et al. Specific targeting of cancer cells by multifunctional mitoxantrone-conjugated magnetic nanoparticles. *J Drug Target* **2013**; 21: 328-40. doi:10.3109/1061186x.2012.750325
24. Barar J, Omidi Y. Dysregulated pH in Tumor Microenvironment Checkmates Cancer Therapy. *Bioimpacts* **2013**; 3: 149-62. doi:10.5681/bi.2013.036
25. Omidi Y, Barar J. Targeting tumor microenvironment: crossing tumor interstitial fluid by multifunctional nanomedicines. *Bioimpacts* **2014**; 4: 55-67. doi:10.5681/bi.2014.021
26. Asgharzadeh MR, Barar J, Pourseif MM, Eskandani M, Jafari Niya M, Mashayekhi MR, et al. Molecular machineries of pH dysregulation in tumor microenvironment: potential targets for cancer therapy. *Bioimpacts* **2017**; 7: 115-33. doi:10.15171/bi.2017.15
27. Xu X, Persson HL, Richardson DR. Molecular pharmacology of the interaction of anthracyclines with iron. *Mol Pharmacol* **2005**; 68: 261-71. doi:10.1124/mol.105.013383
28. Fernandez-Chas M, Curtis MJ, Niederer SA. Mechanism of doxorubicin cardiotoxicity evaluated by integrating multiple molecular effects into a biophysical model. *Br J Pharmacol* **2018**; 175: 763-81. doi:10.1111/bph.14104
29. Olson RD, Mushlin PS, Brenner DE, Fleischer S, Cusack BJ, Chang BK, et al. Doxorubicin cardiotoxicity may be caused by its metabolite, doxorubicinol. *Proc Natl Acad Sci U S A* **1988**; 85: 3585-9.
30. Mordente A, Meucci E, Silvestrini A, Martorana GE, Giardina B. New developments in anthracycline-induced cardiotoxicity. *Curr Med Chem* **2009**; 16: 1656-72. doi:10.2174/092986709788186228
31. Cole SP, Bhardwaj G, Gerlach JH, Mackie JE, Grant CE, Almquist KC, et al. Overexpression of a transporter gene in a multidrug-resistant human lung cancer cell line. *Science* **1992**; 258: 1650-4. doi:10.1126/science.1360704
32. Germann UA. P-glycoprotein--a mediator of multidrug resistance in tumour cells. *Eur J Cancer* **1996**; 32a: 927-44. doi:10.1016/0959-8049(96)00057-3
33. Oakman C, Moretti E, Galardi F, Santarpia L, Di Leo A. The role of topoisomerase IIalpha and HER-2 in predicting sensitivity to anthracyclines in breast cancer patients. *Cancer Treat Rev* **2009**; 35: 662-7. doi:10.1016/j.ctrv.2009.08.006
34. Taylor-Papadimitriou J, Burchell J, Miles DW, Dalziel M. MUC1 and cancer. *Biochim Biophys Acta* **1999**; 1455: 301-13. doi:10.1016/S0925-4439(99)00055-1
35. Raina D, Uchida Y, Kharbanda A, Rajabi H, Panchamoorthy G, Jin C, et al. Targeting the MUC1-C oncoprotein downregulates HER2 activation and abrogates trastuzumab resistance in breast cancer cells. *Oncogene* **2014**; 33: 3422-31. doi:10.1038/onc.2013.308
36. Jafarizad A, Aghanejad A, Sevim M, Metin Ö, Barar J, Omidi Y, et al. Gold Nanoparticles and Reduced Graphene Oxide-Gold Nanoparticle Composite Materials as Covalent Drug Delivery Systems for Breast Cancer Treatment. *ChemistrySelect* **2017**; 2: 6663-72. doi:doi:10.1002/slct.201701178
37. Nagaprashantha L, Vartak N, Awasthi S, Awasthi S, Singhal SS. Novel anti-cancer compounds for developing combinatorial therapies to target anoikis-resistant tumors. *Pharm Res* **2012**; 29: 621-36. doi:10.1007/s11095-011-0645-9
38. Paoli P, Giannoni E, Chiarugi P. Anoikis molecular pathways and its role in cancer progression. *Biochim Biophys Acta* **2013**; 1833: 3481-98. doi:10.1016/j.bbamcr.2013.06.026
39. Cao Z, Livas T, Kyprianou N. Anoikis and EMT: Lethal "Liaisons" during Cancer Progression. *Crit Rev Oncog* **2016**; 21: 155-68. doi:10.1615/CritRevOncog.2016016955
40. O'Connor R. The pharmacology of cancer resistance. *Anticancer Res* **2007**; 27: 1267-72.
41. Kuo MT. Roles of multidrug resistance genes in breast cancer chemoresistance. In: Yu D, MC Hung, editors. *Breast Cancer Chemosensitivity*: Springer; **2007**. p. 23-30.
42. Markman JL, Rekechenetskiy A, Holler E, Ljubimova JY. Nanomedicine therapeutic approaches to overcome cancer drug resistance. *Adv Drug Deliv Rev* **2013**; 65: 1866-79. doi:10.1016/j.addr.2013.09.019
43. Tekchandani P, Kurmi BD, Paliwal SR. Nanomedicine to Deal With Cancer Cell Biology in Multi-Drug Resistance. *Mini Rev Med Chem* **2017**; 17: 1793-810. doi:10.2174/1389557516666160219123222
44. Friberg S, Nystrom AM. NANOMEDICINE: will it offer possibilities to overcome multiple drug resistance in cancer? *J Nanobiotechnology* **2016**; 14: 17. doi:10.1186/s12951-016-0172-2
45. Iyer AK, Singh A, Ganta S, Amiji MM. Role of integrated cancer nanomedicine in overcoming drug resistance. *Adv Drug Deliv Rev* **2013**; 65: 1784-802. doi:10.1016/j.addr.2013.07.012
46. Bhirde AA, Chikkaveeraiah BV, Srivatsan A, Niu G, Jin AJ, Kapoor A, et al. Targeted therapeutic nanotubes influence the viscoelasticity of cancer cells to overcome drug resistance. *ACS Nano* **2014**; 8: 4177-89. doi:10.1021/nn501223q
47. Shapira A, Livney YD, Broxterman HJ, Assaraf YG. Nanomedicine for targeted cancer therapy: towards the overcoming of drug resistance. *Drug Resist Updat* **2011**; 14: 150-63. doi:10.1016/j.drup.2011.01.003
48. Johari-Ahar M, Barar J, Alizadeh AM, Davaran S, Omidi Y, Rashidi MR. Methotrexate-conjugated quantum dots: synthesis, characterisation and cytotoxicity in drug resistant cancer cells. *J Drug Target* **2016**; 24: 120-33. doi:10.3109/1061186x.2015.1058801
49. Rahmanian N, Eskandani M, Barar J, Omidi Y. Recent trends in targeted therapy of cancer using graphene oxide-modified multifunctional nanomedicines. *J Drug Target* **2017**; 25: 202-15. doi:10.1080/1061186x.2016.1238475
50. Saberian M, Hamzeiy H, Aghanejad A, Asgari D. Aptamer-based Nanosensors: Juglone as an Attached-Redox Molecule for Detection of Small Molecules. *Bioimpacts* **2011**; 1: 31-6. doi:10.5681/bi.2011.005
51. Mashinchian O, Salehi R, Dehghan G, Aganejad A, Davaran S, Omidi Y. Novel thermosensitive poly (N-isopropylacrylamide-co-vinylpyrrolidone-co-methacrylic acid) nanosystems for delivery of natural products. *International Journal of Drug Delivery* **2010**; 2.
52. Barar J, Omidi Y. Cellular Trafficking and Subcellular Interactions of Cationic Gene Delivery Nanomaterials. *J Pharm Nutr Sci* **2011**; 1: 61-8. doi:10.6000/1927-5951.2011.01.01.12
53. Altschuler Y, Kinlough CL, Poland PA, Bruns JB, Apodaca G, Weisz OA, et al. Clathrin-mediated endocytosis of MUC1 is modulated by its glycosylation state. *Mol Biol Cell* **2000**; 11: 819-31.
54. Liu X, Yuan Z, Chung M. MUC1 intra-cellular trafficking is clathrin, dynamin, and rab5 dependent. *Biochem Biophys Res Commun* **2008**; 376: 688-93. doi:10.1016/j.bbrc.2008.09.065
55. Hanafi-Bojd MY, Moosavian Kalat SA, Taghdisi SM, Ansari L, Abnous K, Malaekeh-Nikouei B. MUC1 aptamer-conjugated mesoporous silica nanoparticles effectively target breast cancer cells. *Drug Dev Ind Pharm* **2018**; 44: 13-8. doi:10.1080/03639045.2017.1371734
56. Perepelyuk M, Sacko K, Thangavel K, Shoyele SA. Evaluation of MUC1-Aptamer Functionalized Hybrid Nanoparticles for Targeted Delivery of miRNA-29b to Nonsmall Cell Lung Cancer. *Mol Pharm* **2018**; 15: 985-93. doi:10.1021/acs.molpharmaceut.7b00900